Lab on a Chip

View Online
Dynamic Article Links

Cite this: *Lab Chip*, 2011, **11**, 1679

www.rsc.org/loc

METHOD

Flexible casting of modular self-aligning microfluidic assembly blocks†

Sean M. Langelier,[a] Eric Livak-Dahl,‡[a] Anthony J. Manzo,‡[b] Brian N. Johnson,[a] Nils G. Walter[b] and Mark A. Burns*[ac]

Received 18th October 2010, Accepted 10th February 2011
DOI: 10.1039/c0lc00517g

The recent shift among developers of microfluidic technologies toward modularized "plug and play" construction reflects the steadily increasing realization that, for many would-be users of microfluidic tools, traditional clean-room microfabrication is prohibitively complex and/or expensive. In this work, we present an advanced modular microfluidic construction scheme in which pre-fabricated microfluidic assembly blocks (MABs) can be quickly fashioned, without expertise or specialized facilities, into sophisticated microfluidic devices for a wide range of applications. Specifically, we describe three major advances to the MAB concept: (1) rapid production and extraction of MABs using flexible casting trays, (2) use of pre-coated substrates for simultaneous assembly and bonding, and (3) modification of block design to include automatic alignment and sealing structures. Finally, several exemplary applications of these MABs are demonstrated in chemical gradient synthesis, droplet generation, and total internal reflection fluorescence microscopy.

1 Introduction

Microfluidic devices are particularly advantageous for biological analysis[1–5] and high-throughput screening.[6–8] However, despite their financial and scientific benefits (*e.g.* experimental parallelization, reduced reagent consumption, short analysis times, portability, the ability to create bio-mimetic structures[9]), widespread adoption of such devices in the research community has yet to occur. One reason for this may be that a significant gap typically exists between the producers of microfluidic technologies (mainly engineers) and end users, the majority of which reside in the life sciences. The high cost and expertise often required to fabricate custom microfluidic devices,[10] it would seem, remains a sufficient deterrent to those researchers who might otherwise benefit from the technology. As such, the development of technologies which enable custom microfluidic fabrication without demanding substantial investment and/or expertise will go a long way toward closing this gap.

A number of researchers have proposed simpler fabrication methods[11–15] aimed at the elimination of costly and time consuming clean-room lithography. To replace the conventional chrome photomask, for example, Duffy *et al.* introduced the use of high-resolution transparencies.[11] Glennon *et al.* went further, moving to direct printing of the lithographic mold—laser toner, in this case, serving as the fluidic structures.[12] This approach is limiting however, as it only allows for a maximum channel height of ~10 μm which is problematic for some biological applications.[13] Others went further still, creating more topologically diverse molds using solid object printers (SOP).[15] But SOP are not ideal due to the substantial cost of the equipment and their generally limited resolution (~250 μm minimum feature size). A clever technique employing direct printing on shrinkable thermoplastics was recently proposed by Grimes *et al.* and is potentially useful for fabricating channels in the range of 50–100 μm.[14]

Modular architectures utilizing fluidic breadboards and pre-fabricated microfluidic components are a popular development of late.[16–18] This approach, more than any other, is amendable to ubiquitous distribution amongst research scientists as pre-fabricated components would allow for standardization and point of use customization. However, the use of a breadboard places inherent limitations on the flexibility of such systems. Recently, Rhee and Burns developed a modular microfluidic assembly block (MAB) platform[19] using pre-fabricated PDMS blocks. With this approach, non-expert users could assemble fully customizable microfluidic devices within minutes at the point of use. Furthermore, this approach did not require the use of a complex breadboard interface.

Here, we report on an advanced MAB concept employing PDMS blocks with assorted channel geometries that are linked together and bonded to form fully functional microfluidic devices (see Fig. 1). Specifically, we introduce: (1) a flexible ice-cube tray

[a]*Department of Chemical Engineering, University of Michigan, 2300 Hayward St. 3074 H.H. Dow Building, Ann Arbor, MI, 48109-2136, USA. E-mail: maburns@umich.edu; Fax: +1 (734) 763-0459; Tel: +1 (734) 764-2383*
[b]*Department of Chemistry, University of Michigan, Ann Arbor, USA*
[c]*Department of Biomedical Engineering, University of Michigan, 2200 Bonisteel Blvd., Ann Arbor, MI, 48109-2099, USA*

† Electronic supplementary information (ESI) available: SU-8 master mold processing notes; mold replication in silicon processing notes; Fig. S1–S5. See DOI: 10.1039/c0lc00517g/

‡ These authors contributed equally to this work.

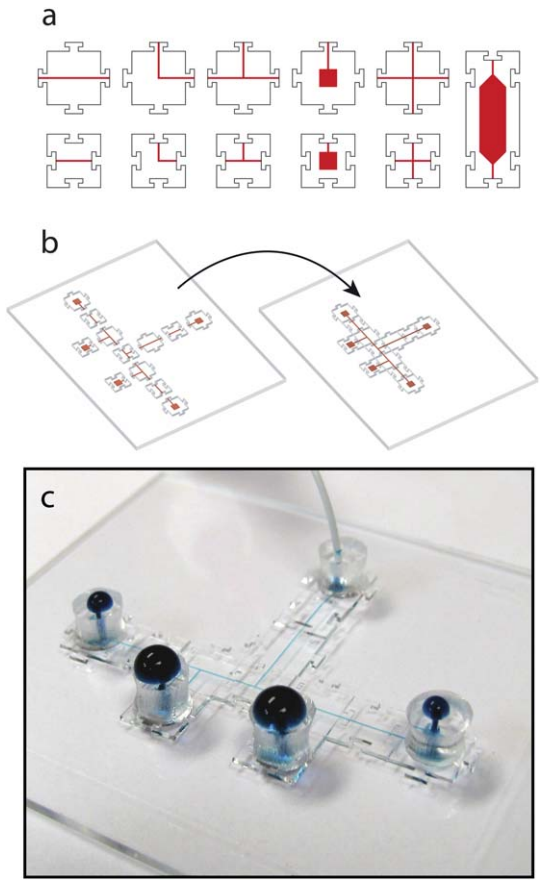

Fig. 1 The MAB concept. (a) Schematic representation of the assorted male and female MABs used in this work. (b) A selection of pre-fabricated MABs prior to (left) and following (right) assembly and bonding. (c) Photograph of actual MAB device, of identical construction, during a flow test.

casting approach which greatly improves the ease and efficiency of the upstream production of MABs by expert practitioners and fabrication foundries, (2) the use of pre-coated assembly substrates and the methodology for their preparation utilizing inexpensive "off the shelf" tools, and (3) a new block design featuring self-aligning structures as well as small radii on the sealing faces of the male MABs for improved sealing at block junctions. The latter two improvements, which are specific to the end user (*i.e.*, the non-expert), enable rapid assembly of MABs into customizable microfluidic devices in just minutes.

2 Materials and methods

2.1 SU-8 master mold preparation

MAB fabrication begins with preparation of master mold structures in SU-8. These precursor SU-8 master molds were constructed in two steps using standard photolithography. First, a thin (50–100 μm) layer of fluidic structures comprising assorted channel geometries was deposited. Second, thicker (250–1200 μm) structures that define the walls of the MABs were added. The fluidic layer of the mold was prepared by spin-casting either SU-8 2025 or SU-8 2035 (MicroChem Corp.) onto bare 4 inch silicon wafers (500 μm thick) to a desired feature height, typically 80 μm. Once coated, wafers were allowed to rest for 5 min before being transferred to a level hotplate with a perforated cover and soft baked for 5 min at 65 °C followed by 20 min at 95 °C, ramping the temperature slowly (2 °C min^{-1}) to ensure smooth solvent evolution. After cooling to room temperature, edge beads were removed by gentle application of a clean room swab soaked in EBR-PG (MicroChem Corp.) with wafers rotating at 500 RPM. De-beaded wafers were exposed on a contact aligner for ~25 s (500–750 mJ cm^{-2}) against a chrome photomask containing the fluidic features (see ESI Fig. S1a†) and allowed to rest for 30 min before undergoing a post-exposure bake at 65 °C for 3 min and 10 min at 95 °C, again gently ramping the temperature up and down on a hotplate with a perforated cover. Once cool, wafers were submersion developed in fresh SU-8 Developer (MicroChem Corp.), rinsed with IPA, and gently blown dry with compressed air or nitrogen.

Mold walls were prepared in a similar fashion, by spin-casting SU-8 2150 (MicroChem Corp.) directly on top of the fluidic structures just described. Spun films were covered and allowed to settle on a level surface for approximately 1 h prior to soft baking. Trapped bubbles in the resist film that were not liberated during the rest period were coaxed out of the resist film by heating the wafers for approximately 30 min in a solvent rich environment, *i.e.*, completely covered with a glass dish, to 65 °C. Any remaining bubbles were ruptured manually, replacing the glass dish as necessary to maintain a solvent rich air/resist interface. Bubble free resist films were subsequently soft baked at 95 °C for approximately 7 h, again ramping the temperature slowly (2 °C min^{-1}). Once cool, edge beads were carefully removed using the procedure described above. Following the soft bake, wafers were aligned to a chrome photo-mask patterned with the assembly block walls (ESI Fig. S1b†) and exposed. For example, an approximately 500 μm film was exposed for 90 s or 2300 mJ cm^{-2}. Wafers were then allowed to rest for 30 min prior to undergoing a low temperature post-exposure bake at 55 °C for 2 h, during which time a very slow temperature ramp (1 °C min^{-1}) is utilized, in order to minimize internal stress in the final SU-8 structures.[20] After returning to room temperature, the wafers were submersion developed for 20–30 min (depending on the film thickness), rinsed with IPA, then DI water, and allowed to air dry. Molds were subsequently treated with O_2 plasma and placed in an evacuated vessel along with 20 μL of tridecafluoro-1,1,2,2-tetrahydrooctyl-1-trichlorosilane for 1 h. A complete schematic representation of SU-8 master mold preparation is shown in ESI Fig. S2†.

2.2 Mold replication in silicone

Durable and flexible silicone replicates of the SU-8 master molds were fabricated using a commercially available low-viscosity liquid silicone rubber (CopyFlex - MYOM, Cincinnati, OH) with a working time of approximately 4 h. Completed SU-8 master molds were placed in a casting tray and encapsulated with the two-component CopyFlex® liquid silicone, prepared according to the manufacturers recommendations. To ensure an accurate and void free mold impression, the encapsulated molds were subjected to 30 inch vac. mercury for 10–20 min. Subsequently, the molds were baked in an oven at approximately 80 °C for 2 h. Once cool, a perfect positive (+) impression of the master mold

was recovered by gently peeling away the cured silicone, which releases effortlessly as a result of the silane treatment discussed above. Failure to silanize the SU-8 precursor resulted in unwanted bonding and often destruction of the master mold. The negative (−) impression of the SU-8 structures was recovered by a repetition of the same silanization and encapsulation procedure just described ending with the silanization of the recovered negative.

2.3 Assembly block casting

Large populations of defect free MABs were rapidly produced by casting ~9 : 1 (base : catalyst, by weight) mixture of PDMS (Sylgard 184, Dow Corning) within the recessed wells of the final silanized silicone molds. The casting procedure was performed by applying an amount of PDMS sufficient to cover the entire mold to a height just above the mold surface. The covered mold was then placed in 30 inch vac. mercury for ~5 min or until a quiescent, bubble-free, PDMS film was observed. Then, using a standard razor blade and applying a modest amount of pressure, excess PDMS was slowly drawn off the mold surface. The best results were achieved by sweeping the razor blade diagonally across the mold furrows with the blade angled slightly in the direction of travel (~30–45°). Due to slight compression of the silicone surface during this procedure (necessary to minimize residual PDMS at the top of the mold walls) it was often necessary to backfill some of the wells. These wells were easily identifiable in good light due to their concave liquid surfaces. Backfilling of wells was accomplished by loading ~200 μL of PDMS into a 1000 μL micropipette tip, removing the tip from the micropipette and using the semi-filled tip as a capillary restrained liquid hopper. Once filled, the mold was placed in an oven for approximately 1–2 h at 80 °C. Cured MABs were then readily removed by flexure of the mold and extraction with dull tweezers. Using this procedure, virtually every usable MAB (wells at the periphery of the mold are often useless as a result of the edge bead removal) was routinely extracted without damage to either the mold or blocks in a matter of minutes.

2.4 Substrate preparation

To prepare a given substrate, a liberal amount of PDMS (1 : 1) was dispensed onto the glass surface. Then, this liquid was spread into a thick film by slowly walking a jet of compressed air or nitrogen in a steady zigzagging pattern over the entire length of the substrate with the jet situated at ~30–45° relative to the substrate surface. The jet was formed using a simple compressed air gun with on/off toggle fitted with a 2 mm ID nozzle (~1 cm in length) in conjunction with a coarse upstream pressure regulator and gauge. This procedure was repeated until an advancing liquid front was no longer visible on the substrate surface. For a 2 × 1 inch glass slide, this took approximately 1 min. After the thin-film was spread, substrates were then allowed to rest for 5–10 min prior to MAB assembly.

2.5 Device assembly

Devices were assembled in a stepwise fashion, on pre-coated glass substrates, by linking the MABs necessary to realize a given design using a pair of fine point tweezers. Scotch tape (3M Corp.) was used to remove dust and particulates from the channel side of the MABs prior to use and a standard stereoscope was used, although not required, as a visual aid during the assembly process. Linking of blocks was greatly facilitated by placing the MABs, insofar as possible, directly in their desired location. A preferred approach was to lean the connecting end of the MAB on the relevant block then depress the alignment keys until the channel side of the block made contact with the liquid film. Once seated, it was typically necessary to press on the block surface to liberate any air bubbles that may have become trapped. This process was repeated, periodically checking the overall alignment, until the target design was realized. Following assembly, completed devices were transferred to a 140 °C hotplate to cure for ~5 min. Once cooled, PDMS posts for fluidic interfacing were affixed to inlet/outlet MABs using a straightforward stamp and cure approach or, optionally, O_2 plasma bonding. Leaks, if present, were quickly repaired by simply returning the device to the 140 °C hotplate and applying a very small amount of PDMS (1 : 1) to the effected junctions. For high pressure applications or if a more robust device was desired, bonded MAB assemblies were fully encapsulated in a thick layer of PDMS (10 : 1).

2.6 Total internal reflection fluorescence microscopy

The total internal reflection fluorescence microscopy (TIRFM) setup consisted of an Olympus IX-81 microscope with a 60× 1.45 NA oil immersion objective (see Fig. 9b), with TIRFM excitation provided by a 532 nm continuous-wave laser (Coherent Compass 315M, 100 mW) fiber-optically coupled into the microscope *via* an Olympus Cell^TIRF module. A Cy3 filter set (Chroma 41007a Cy3TM®) was used for data collection, consisting of a Chroma HQ545/30× exciter, Q570LP dichroic, and HQ610/75 emitter. Laser power was adjusted using an acousto-optical tunable filter (AOTF) and excitation alignment and incident angle adjustment were accomplished using the Cell^TIRF module. Images were recorded with a Photometrics Evolve EMCCD. Nanospheres used for TIRFM were red fluorescent, 200 nm diameter FluoSpheres F8810 (Molecular Probes) with excitation/emission peaks of 580/605 nm.

3 Results and discussion

3.1 SU-8 fabrication

SU-8 master molds were constructed using a multi-step photolithographic approach. Completed molds consisted of thin fluidic structures (typically 80 μm), with a variety of channel designs, and thick walls (typically 250–500 μm) that defined the periphery of the MABs. Adjustment of channel and wall dimensions were possible by alteration of spin speed, use of alternate SU-8 formulations, or by the successive addition of multiple spin and bake cycles.[19] SEM images of two completed master molds are shown in Fig. 2a and 2b. Final SU-8 structures possessed very smooth sidewalls with sharply defined boundaries—two features critical to the quality of inter-block alignment and sealing. A slightly negative or overhanging pitch to the SU-8 sidewalls (Fig. 2c) was typically observed regardless of the mold wall thickness. This phenomenon results from the use of a broadband UV source on the contact aligner and could be eliminated by installation of a long-pass filter to block UV transmission below

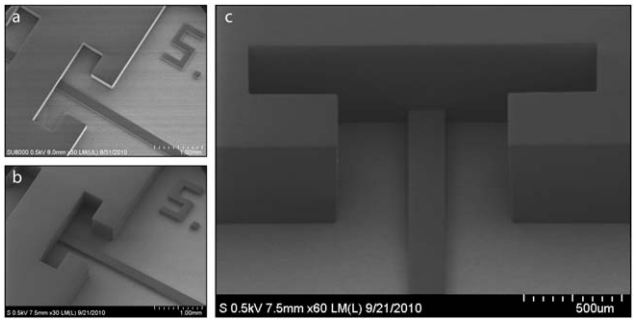

Fig. 2 SEM images of precursor SU-8 master molds. (a) Mold with ~250 μm thick walls and 80 × 200 μm fluidic channels. (b) Mold with ~500 μm thick walls and 80 × 200 μm fluidic channels. (c) Image of mold in (b) illustrating the negative pitch or sidewall irregularity that was typically observed.

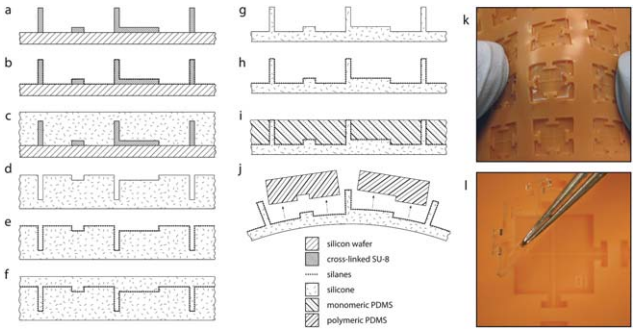

Fig. 3 Schematic representation of replication of SU-8 master molds in flexible silicone. (a) Pre-cursor master mold constructed from SU-8 on a 4 inch silicon wafer. (b) Chemical surface modification of (a) with trichlorosilanes. (c) Encapsulation of (b) with liquid silicone. (d) Positive silicone cast following release. (e) Chemical surface modification of (d) with trichlorosilanes. (f) Encapsulation of (e) with liquid silicone. (g) Recovery of negative silicone cast following release. (h) Chemical surface modification of (g) with trichlorosilanes. (i) Filling of MAB wells with PDMS monomer. (j) Following PDMS polymerization, MABs are released by flexure of the silicone mold. (k) Image of actual 250 μm silicone mold during step (j). (l) Extraction of a male MAB using a pair of blunt tweezers.

350 nm. Sidewall overhang manifests itself, in this case, as V-shaped crevices between adjacent MABs. The consequence of this, depending upon the severity of the overhang, are inter-block gaps that potentially extend to the channel floor.

It is worth noting that thick SU-8 processing was made particularly difficult by the development of high internal stresses in the final cross-linked epoxy. For SU-8 structures thicker than ~250 μm it was common to experience—even with careful preparation—severe cracking, de-lamination, substrate deformation, and resist distortion. These issues were all but eliminated after implementing a protocol similar to one developed by Li *et al.* who used extended soft bake times, lower post-exposure bake temperatures, and slow temperature ramping in order to achieve final SU-8 structures with 70% less internal stress and 50% greater tensile strength.[20]

3.2 Flexible casting trays

MAB extraction from rigid SU-8 master structures requires the delicate use of sharp tools such as syringe needles or razor blades;[19] however, even with great care, it is difficult to avoid gouging the sidewalls of the SU-8 and/or damaging the MABs themselves in the process. To address this, we developed a casting approach that facilitates MAB extraction while also preserving the integrity of the SU-8 masters. The approach, illustrated in Fig. 3a–3j, utilizes a low-viscosity liquid silicone rubber to create near-perfect—some benign surface roughening was observed (see supplementary Fig. S3†)—replicates of the original SU-8 master structures. Silicone rubber replicates are highly flexible and durable, allowing for the production of MABs with greater rapidity and ease without causing damage to costly SU-8 master structures.

Chemical treatment of the silicone replicates with trichlorosilanes was found to yield a passivated surface that did not bind to PDMS. MAB extraction, as such, was trivially performed by flexing the casting tray and extracting the MABs with a pair of dull tweezers (see Fig. 3k and 3l). With this process, it was common to harvest an entire trays worth of MABs (50–60 blocks) with nearly 100% success in only minutes, and hundreds of MABs within a few hours. By contrast, the extraction of a comparable number of MABs directly from SU-8 master structures took approximately 2 h with a success rate of approximately 70–80%. An additional benefit to this approach is that it affords other opportunities for potential end users, namely, the option to make their own supply of MABs.

Some thickness variation among extracted MABs was observed. These variations (>100 μm in some cases) arose from insufficiently leveled hot plates during the soft bake and post exposure bake steps of the lithography. Female MABs were found to be thicker, on average, than males regardless of master mold thickness (see ESI Fig. S4†). This difference in overall piece thickness reflects the consistent orientation with which the wafers were placed on the hotplates. Note that these variations did not appear to effect the performance of planar MAB assemblies. However, such variations would inhibit realization of three-dimensional, multi-layer, MAB devices. Development of multi-layer MAB structures is the subject of ongoing work and will allow for more advanced microfluidic components such as peristaltic pumps, valves, and fluidic logic structures[21,22] to be created in the same manner as a planar MAB device.

3.3 Block design

Abrupt deviations in channel cross-section and/or flow direction can pose problems for microfluidic systems by introducing sharp pressure drops and small pockets of stagnation in the flow. Thus, the fabrication method used should yield devices with reliable hydraulic diameters. Toward this end, MABs were modified to include jigsaw-like lock and key (male and female) structures (Fig. 4a). These structures fix the relative orientations of neighboring MABs thus ensuring both local and long range alignment of the fluidic network. The sealing face of the male MABs were also modified to include very small trapezoidal extensions (henceforth referred to as the piece *convexity*) of 0, 2, 5, and 10 μm (see δ, in Fig. 4a). Alignment and offset data for numerous MAB junctions at each convexity is shown in Fig. 4b. Detailed statistics of channel offset and alignment angle are plotted in

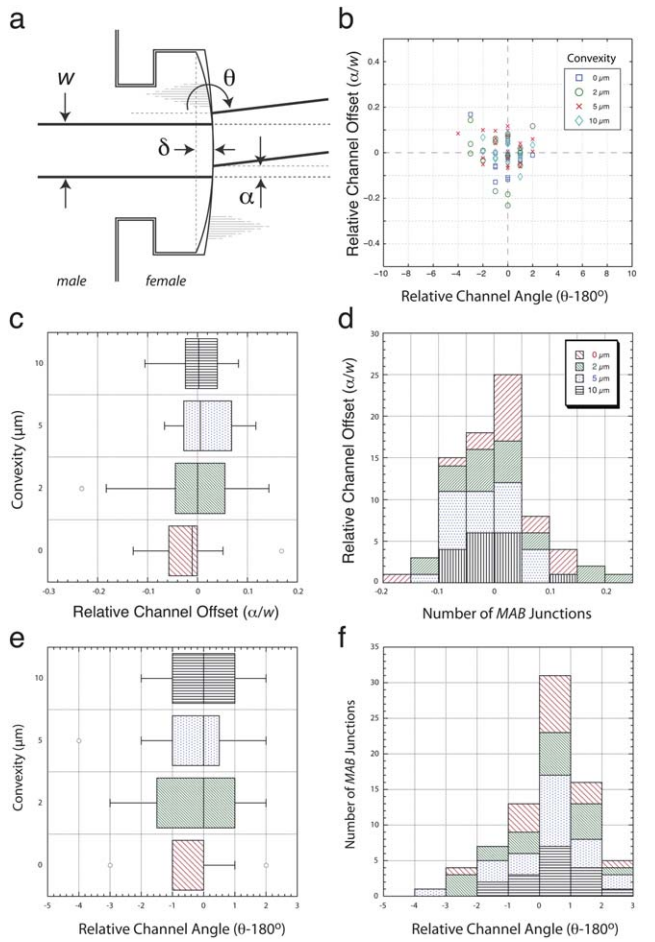

Fig. 4 Channel alignment and offset statistics for a random sampling of MAB junctions with various piece convexities. (a) Schematic illustration of a MAB junction highlighting relevant parameters: channel width (w), channel offset (α), channel angle (θ), piece convexity (δ). (b) Bulls-eye plot of relative channel offset (α/w) and relative channel angle ($\theta-180^\circ$) for ≥20 MABs at each convexity. (c) Box plot of relative channel offset *versus* piece convexity. (d) Histogram of (c). (e) Box plot of relative channel angle *versus* piece convexity. (f) Histogram of (e).

Fig. 4c–4f. The interquartile range of the relative channel offset (α/w), for example, was found to be ±0.06 with a maximum recorded offset of ~0.2. Similarly, the relative channel angle ($\theta-180^\circ$) was found to be approximately ±1.0° with a maximum angle deviation of 3.0–4.0°. Note that channel offset and angle do not appear to be a function of piece convexity; however, the data for 0 μm convexity displays the tightest range in each case.

Elimination of inter-block gaps is important to the functionality of completed MAB devices. To minimize the occurrence of inter-block gaps (mathematically defined as the distance between two blocks at the channel roof) varying amounts of convexity were added to the sealing face of the male pieces. By incorporation of this additional material, it was thought that the sealing faces of two linked MABs would be held in a state of increased compression, thus decreasing the likelihood of gaps forming. Moreover, it was thought that the presence of these minuscule PDMS cushions would compensate for the V-shaped crevices resulting from the negatively sloping sidewalls in the master structures mentioned above. Strangely, a sampling of bonded

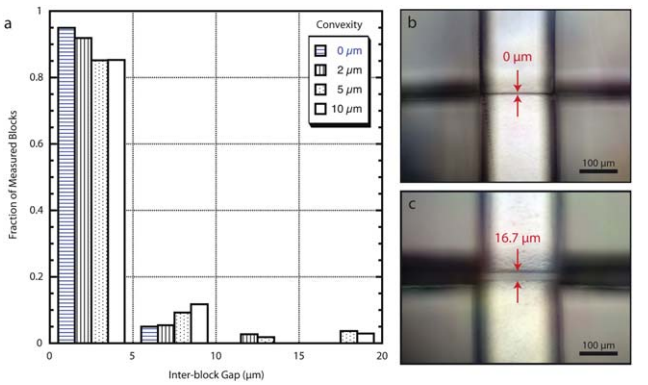

Fig. 5 Inter-block gaps for a sampling ($N \geq 20$ in each case) of bonded MABs with different piece convexity. (a) Histogram of inter-block gap magnitudes for assembled and bonded MABs of various convexity (four bins: 0–5 μm, 5–10 μm, 10–15 μm, and 15–20 μm). (b) Microscope image of a 0 μm gap. (c) Microscope image of a 16.7 μm gap.

MAB junctions at each convexity indicates that an increase in convexity results in an increase of both the frequency and the magnitude of the observed inter-block gaps (Fig. 5a). Despite this somewhat counterintuitive result, the vast majority of sampled junctions (>80%, regardless of convexity) exhibit inter-block gaps of ≤5 μm; and within that group, the fraction of junctions displaying no gaps were 80%, 60%, 56%, and 56% for convexities of 0, 2, 5, and 10 μm, respectively. For illustrative purposes, a pair of such junctions with 0 μm and 16.7 μm gaps are shown in Fig. 5b and 5c, respectively.

3.4 Substrate preparation

Researchers often take advantage of the native stiction of PDMS in the design and construction of microfluidic systems. Stiction is problematic, however, when attempting to precisely position arrays of objects in close proximity to one another. For MABs, such a scenario is particularly undesirable because poor positioning of the blocks leads to non-functional devices. As such, we developed a simple means of preparing glass substrates for MAB assembly by coating them with thin-films of PDMS monomer. Our thin-films, the thickness of which is tunable over a range of 1–3 μm, serve as a lubricating layer upon which MABs can freely glide, allowing linked assemblies of MABs to settle into tight low-stress configurations. The thin liquid films have the added benefit of wicking up into the interstitial spaces between blocks allowing for covalent lateral linkage of the MABs during the heat cure step.

Preliminary determination of the optimal film thickness was accomplished by performing MAB assembly on a series of spin-coated (1 : 1) films with thicknesses of 2–22 μm. Note that the MABs used possessed channel depths of 60–80 μm. A film of ~2 μm (6000 RPM, 30 s) was found to be of sufficient liquidity to allow facile manipulation of the MABs and capillary wicking of PDMS into the block gaps, but was thin enough so that the fluidic channels did not readily flood during a routine assembly. However, because the purchase of a spin-coater is likely not feasible for most end users, numerous "*off the shelf*" methods were explored in an effort to reproduce the characteristics of the 6000 RPM spun films. The average thickness and deviation for

films prepared by: spin coater at 6000 RPM, 40 psi compressed air, hand application with a clean room wipe, a razor blade drawn over bare glass, and a razor blade drawn over various etched glass recesses is plotted in Fig. 6a. Of these methods, the use of a compressed gas jet was found to be superior, yielding films with a thickness and deviation comparable to those of the spin coated benchmark films. Etched glass recesses, though ultimately effective in producing the target film thickness suffered from poor uniformity, most likely due to the unavoidable deflection of the razor blade, and required the use of hazardous chemical etchants.

The compressed gas approach was further refined by addition of coarse pressure regulator allowing for controllable film thickness in the range of 1–3 μm. Fig. 6b shows the resulting film thickness and associated standard error for substrates prepared by walking a compressed air jet in a zigzagging pattern (*inset*, Fig. 6b) with gas pressures over the range of 40–80 psi. Ideal results for the MAB dimensions utilized here were achieved with an upstream gas pressure of ~60 psi (measured under fully open flow conditions). It is worth noting that some minor variation along the substrate length, specifically a slight increase in thickness toward the substrate edge, was observed (ESI Fig. S5†) using this technique. It is also worth noting that the optimal thin-film thickness should cater to the channel dimensions of the MABs being used. MABs with fluidic features on the order of a few microns, for example, might require a thin-film prepared by drawing a razor blade over bare glass.

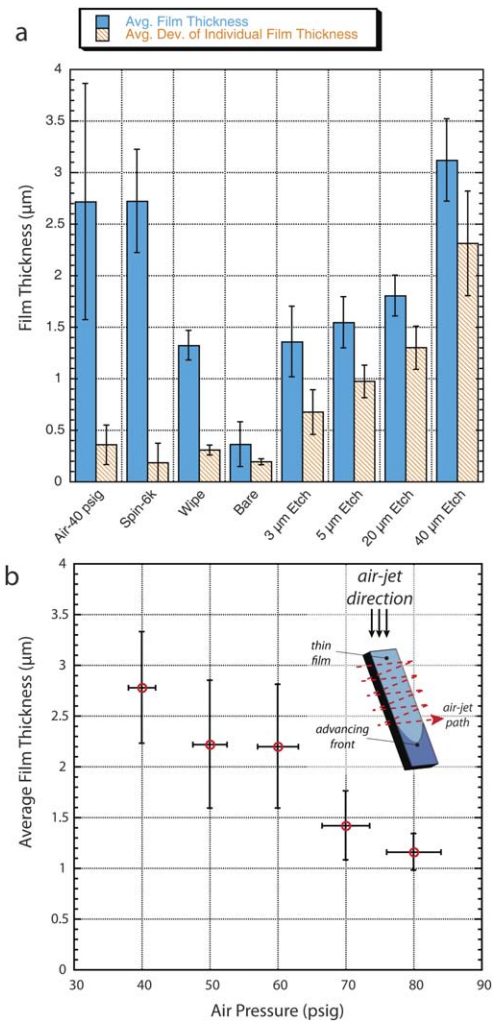

Fig. 6 Summary of "off the shelf" methods for the preparation of PDMS thin-films. (a) Resulting average film thickness and variation for assorted preparation methods. (b) Film thickness calibration plot for preparation using a compressed air jet (see *inset*).

3.5 Assembly and bonding

Condensation of the assembly and bonding steps of the MAB process greatly simplifies device construction. During assembly, the blocks float on a lubricating thin-film of PDMS monomer, enabling facile linkage, and allowing the blocks to settle into close, low-stress contact. Simultaneously, the PDMS film acts as a liquid reservoir, filling the interstitial gaps between MABs by capillary action (*inset*, Fig. 7a). The ~80 μm MAB channels used in this work were sufficiently large compared to the PDMS film thickness so as to provide some leeway when sliding or reorienting a device during assembly. It is worth noting, however, that excessive sliding did result in a flooded channel. When this happened the effected MAB(s) were simply removed and replaced with fresh blocks. Capillary re-distribution of the thin liquid film was not observed to be a problem in such cases.

Lateral and surface bonding of MAB assemblages occurs in minutes after placement on a 140 °C hotplate. Fig. 7b–7d show SEM cross-sections of some example MAB devices following this bonding step. Note that the block interfaces have formed a continuum as a result of the capillary penetration of the PDMS liquid film. Finished devices, which are essentially PDMS monoliths following the heat treatment, can be used immediately upon removal from the hotplate. Leak free 250 μm MAB devices could routinely withstand liquid pressures in excess of 15 psi

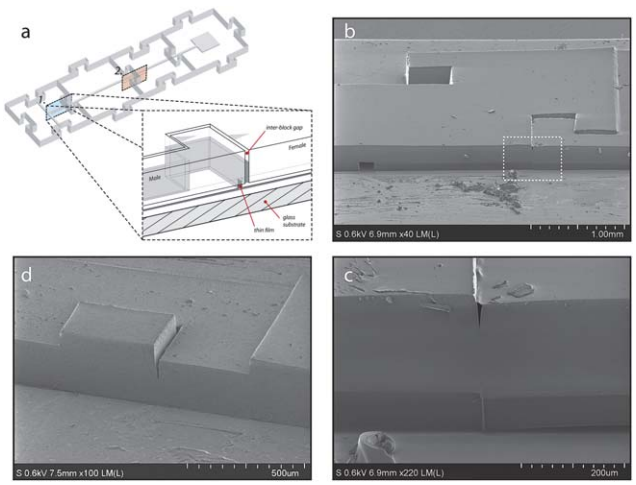

Fig. 7 (a) Schematic illustration of an assembled MAB device and detail (*inset*) of the device cross-section shown by plane No. 1 highlighting the capillary wicking of the liquid film into the inter-block gap. (b) Companion SEM image of the cross-section defined by plane No. 1 in an actual MAB device with the same channel geometry. (c) Close-up of the highlighted rectangle in (b) showing the bond which has formed at the MAB junction well above the channel roof. (d) Companion SEM of plane No. 2 in (a) showing the vertical bond penetration extending from the substrate surface ~150 μm.

(more than adequate for most microfluidic applications). Note that inter-block and block-substrate junctions are highly cross-linked PDMS owing to the 1 : 1 formulation of the PDMS thin film. However, interfacial bonding between blocks, especially at the channel roof, is not always pristine and may contain small gaps and/or weak spots which can rupture under high pressures. Thus, for higher-pressure operation (>5–10 psi) or simply when a more robust device was desired, finished MAB devices were encapsulated in a thicker (~0.5–1 cm) layer of PDMS—a trivial operation—resulting in a finished monolithic device that is virtually indistinguishable, in performance and appearance, to one produced using conventional soft lithography.

Leaks were occasionally observed during fluidic testing of finished MAB devices owing to the presence of inter-block gaps, but were easy to fix. When present, leaks were invariably found to occur at an inter-block junction and always vertically upward through the V-shaped crevice between pieces. It is important to note that in such cases the utility of the device was rarely lost. In fact, the repair of leaks was found to be quick and straightforward. Such a device was simply returned to the 140 °C hotplate and a small amount of PDMS (1 : 1) was applied on the effected junctions using a loaded micropipette tip. The polymerization time, given the small amount of PDMS and the high catalyst ratio, was on the order of a few seconds. Thus even relatively large inter-block gaps (~20 μm) were routinely repairable as the PDMS, which rapidly fills the inter-block region, polymerizes before any channel flooding could occur.

4 Exemplary applications of MAB devices

4.1 Chemical gradient synthesis

Fine spatial control of chemical gradients is helpful in the study of cellular populations, where it is often desirable to probe for toxicity limits over a wide range of concentrations. Using a traditional experimental approach, this would require preparation of a series of dilutions and simultaneous monitoring of a number of experiments in parallel. The same task is made far simpler in a microfluidic system with the aid of a chemical gradient generator. Such a device produces a spatial concentration gradient spanning the transverse dimension of a given micro-channel and can be finely tuned by adjusting inlet flow ratios. Using this approach, a continuum of toxicity data could conceivably be obtained in a single compact experiment.

The layout for a two-component version of such a device constructed from 58 MABs is shown in Fig. 8a. The finished device, which has been encapsulated in PDMS for durability, along with gradient data generated by the device across the path M–M are shown in Fig. 8b and 8c, respectively. Note the long-range alignment of the fluidic channels and the smooth nearly linear variation in the generated gradient.

4.2 Droplet generation

Among its many documented applications, microfluidic droplet generation is very attractive as a means of culturing microbial consortia, where symbiotic nutrient exchange between constituent members is poorly understood. In a microfluidic setting, thousands of uniformly sized droplets containing a probabilistic distribution of unknown species can easily be generated in

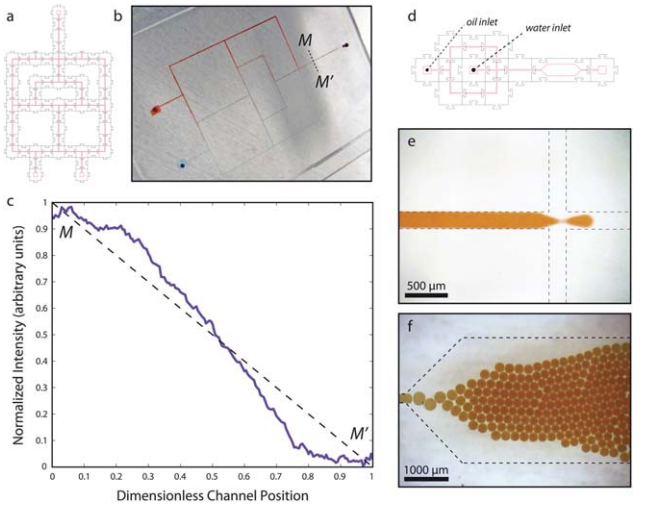

Fig. 8 Chemical gradient and droplet generation in MAB devices. (a) Schematic of two component chemical gradient generator constructed from 58 MABs. (b) Image of completed MAB device following additional encapsulation in PDMS. (c) Pixel intensity plot illustrating the sigmoidal variation of the generated gradient along the path M–M′ in (b). (d) Schematic of 13 block flow-focus droplet device. (e) Close-up image of the device in (d) during operation illustrating the formation of a water droplet at the flow-focused junction (dotted lines are to illustrate channel boundaries). (f) Close-up image of the device in (d) during operation showing the generation and accumulation of highly stabilized and uniform droplets in the downstream chamber (dotted lines are to illustrate channel boundaries).

seconds. The sequestered droplets could then be incubated and later screened for symbiotic interactions. This form of high throughput screening requires narrow tolerances on the sizes of generated droplets as well as stability of the resulting emulsion.

Construction of such droplet devices is straightforward with MABs. Fig. 8d shows an example of a simple flow-focusing droplet generator consisting of 12 standard MABs and 1 custom droplet collection/cultivation block. Images of the working device, after additional PDMS encapsulation to reinforce the large thin diaphragm of the droplet chamber, are shown in Fig. 8e and 8f. A speciality surfactant (RainDance Technologies, Inc.) was used to stabilize the generated droplets which can be packed into the droplet chamber and incubated for greater than 24 h without coalescence—a necessary characteristic for bio-cultivation.

4.3 Total internal reflectance microscopy

TIRFM is an indispensable experimental technique for studying the dynamics of single molecules.[23] For single molecule researchers, particularly in the biological sciences, the most common method for imaging and probing their samples is to add them between a microscope slide and cover glass. Simple custom micro-channels are then often created using, for example, double-sided tape, wax, or Parafilm® for spacing. Holes can be drilled into the microscope slide to allow for pipetting, or to attach tubing to allow for fluidic delivery of reagents and buffers. MABs offer a far more precise and versatile means of fabricating these custom micro-channels, as blocks with user defined

dimensions are very easily assembled at the point of use and afford users options for flow and sample manipulation not possible with conventional approaches.

To demonstrate the use of MABs for objective-based TIRFM (Fig. 9a) imaging was performed with small fluorescent nanospheres and single fluorophore molecules. Single channel MAB devices were constructed on a microscope cover glass (Fig. 9b). During TIRFM, most nanospheres (200 nm in diameter, suspended in a dilute water solution) were found to be in a state of Brownian motion; however, many others were found adsorbed to the PDMS block surfaces or the ~2 μm layer of PDMS on the coverslip (deposited to aid MAB bonding). The evanescent light field due to the TIRFM conditions was readily apparent by comparing emission of bright—due to their proximity to the evanescent TIRFM field—surface-bound beads with that of dim, freely diffusing beads further away from the surface (Fig. 9c). Adjusting the illumination angle to allow for epi-illumination resulted in the freely diffusing beads also becoming bright, and their diffusion paths could be observed for extended periods of travel so long as they remained near the focus of the microscope.

Additionally, objective-based TIRFM illumination was verified by measuring the emission intensity from the surface-bound beads as the incident TIRFM angle was adjusted over a range of angles. The incident angle was adjusted by positioning the excitation beam relative and parallel to the objective lens axis. Measurements of bead emission *versus* incident angle revealed the expected characteristic theoretical curves[24,25] for TIRFM intensity *versus* incidence angle. There is a rise in emission intensity when the incident angle approaches the critical angle, mainly caused by a type of partial, highly oblique epi-illumination near subcritical angles,[26,27] and a decay as the angle is further increased past the critical angle. We found the critical angle for the PDMS coated coverslip to be ~1 to 2 degrees larger than the critical angle for a simple coverslip/buffer interface due to the micron thin layer of PDMS affecting the true critical angle and excitation intensity.[24,28] Our results show excellent promise for the use of MABs in many applications where imaging at the PDMS/buffer interface is needed. Similar experiments for prism-based TIRFM were also performed (data not shown), except no adjustments in TIRFM excitation angle were made.

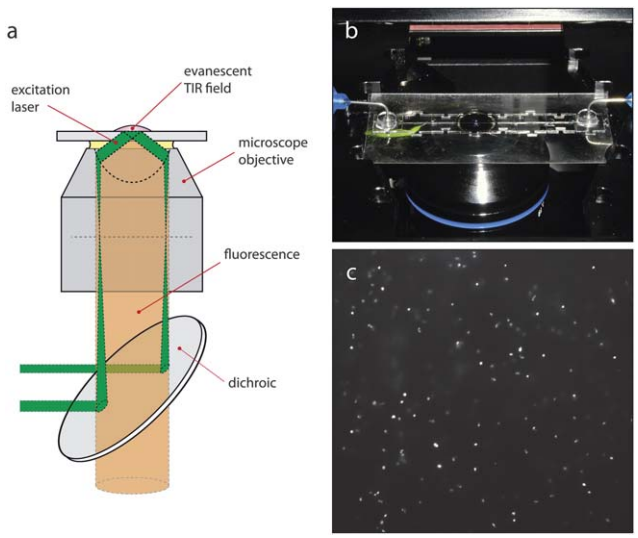

Fig. 9 TIRFM using MAB devices. (a) Simplified schematic of objective-based TIRFM. (b) Image of 7-block straight channel MAB device, with attached fluidic inputs, on the TIRFM stage. (c) Image from objective-based TIRFM excitation, illustrating the difference in signal from surface-bound (bright) and freely diffusing (dim) 200 nm nanospheres.

5 Conclusions

The MAB approach presented is a simple and inexpensive alternative to traditional microfabrication techniques and is aimed at closing the gap between the developers of microfluidic technologies and the core potential user base in the life sciences. Anyone, regardless of discipline, can quickly assemble these building blocks into sophisticated microfluidic devices according to their own designs. In this work, we discussed several advancements to the original MAB concept[19] including: the use of flexible molds for improved casting and extraction of MABs, the modification of the block design to include auto-alignment structures, analysis of the effectiveness of added material to the male structures for improved sealing, and the use of pre-coated substrates for condensing the assembly and bonding steps of the process. Exemplary MAB devices were also presented to illustrate that the technology could be readily applied to a variety of scientific applications. The MAB platform has no intrinsic limitations on the channel layouts or block dimensions used. Future users of MABs could work with fabrication foundries to develop custom sets of blocks to suit their specific needs. Simplified MAB production using flexible silicone molds affords users the additional option of producing their own supply of MABs. Optimization of precursor mold lithography will allow for MABs with highly uniform thickness and perfectly vertical sidewalls. Perfectly vertical sidewalls could eliminate inter-block gaps, and by extension, the need to repair leaks. Such improvements would enable the construction of multi-layer MAB devices with more advanced structures such as pneumatic control and fluidic logic.

Acknowledgements

The authors thank Nick Schuelke (University of Michigan, Ann Arbor) for his valuable assistance in the early stages of this work. Photolithography presented in this work was completed at both the Lurie Nanofabrication Facility (University of Michigan, Ann Arbor) and the Chemical Engineering Clean-Room (University of Michigan, Ann Arbor). This work was partially funded by: NIH 5 R01 EB006789, 5 R01 AI049541 and NSF CBET 0707383.

References

1 J. El-Ali, P. Sorger and K. Jensen, *Nature*, 2006, **442**, 403–411.
2 M. A. Burns, *Science*, 2002, **296**, 1818–1819.
3 D. Meldrum and M. Holl, *Science*, 2002, **297**, 1197.
4 M. Burns, B. Johnson, S. Brahmasandra, K. Handique, J. Webster, M. Krishnan, T. Sammarco, P. Man, D. Jones and D. Heldsinger, *et al.*, *Science*, 1998, **282**, 484.
5 R. Pal, M. Yang, R. Lin, B. Johnson, N. Srivastava, S. Razzacki, K. Chomistek, D. Heldsinger, R. Haque and V. Ugaz, *et al.*, *Lab Chip*, 2005, **5**, 1024–1032.
6 J. Agresti, E. Antipov, A. Abate, K. Ahn, A. Rowat, J. Baret, M. Marquez, A. Klibanov, A. Griffiths and D. Weitz, *Proc. Natl. Acad. Sci. U. S. A.*, 2010, **107**, 4004.

7 P. Hung, P. Lee, P. Sabounchi, R. Lin and L. Lee, *Biotechnol. Bioeng.*, 2005, **89**, 1–8.
8 M. McClain, C. Culbertson, S. Jacobson, N. Allbritton, C. Sims and J. Ramsey, *Anal. Chem.*, 2003, **75**, 5646–5655.
9 D. Huh, B. Matthews, A. Mammoto, M. Montoya-Zavala, H. Hsin and D. Ingber, *Science*, 2010, **328**, 1662.
10 G. Whitesides, *Nature*, 2006, **442**, 368–373.
11 D. Duffy, J. McDonald, O. Schueller and G. Whitesides, *Anal. Chem.*, 1998, **70**, 4974–4984.
12 A. Tan, K. Rodgers, J. Murrihy, C. O'Mathuna and J. Glennon, *Lab Chip*, 2001, **1**, 7–9.
13 A. Liu, F. He, K. Wang, T. Zhou, Y. Lu and X. Xia, *Lab Chip*, 2005, **5**, 974–978.
14 A. Grimes, D. Breslauer, M. Long, J. Pegan, L. Lee and M. Khine, *Lab Chip*, 2008, **8**, 170–172.
15 J. McDonald and G. Whitesides, *Acc. Chem. Res.*, 2002, **35**, 491–499.
16 K. Shaikh, K. Ryu, E. Goluch, J. Nam, J. Liu, C. Thaxton, T. Chiesl, A. Barron, Y. Lu and C. Mirkin, *et al.*, *Proc. Natl. Acad. Sci. U. S. A.*, 2005, **102**, 9745.
17 P. Yuen, *Lab Chip*, 2008, **8**, 1374–1378.
18 P. Grodzinski, J. Yang, R. Liu and M. Ward, *Biomed. Microdevices*, 2003, **5**, 303–310.
19 M. Rhee and M. Burns, *Lab Chip*, 2008, **8**, 1365–1373.
20 B. Li, M. Liu and Q. Chen, *J. Microlithogr., Microfabr., Microsyst.*, 2005, **4**, 043008.
21 M. Rhee and M. Burns, *Lab Chip*, 2009, **9**, 3131.
22 B. Mosadegh, C. Kuo, Y. Tung, Y. Torisawa, T. Bersano-Begey, H. Tavana and S. Takayama, *Nat. Phys.*, 2010, **6**, 433–437.
23 N. Walter, C. Huang, A. Manzo and M. Sobhy, *Nat. Methods*, 2008, **5**, 475–489.
24 D. Axelrod, *Methods Enzymol.*, 2003, **361**, 1–33.
25 A. Mattheyses and D. Axelrod, *J. Biomed. Opt.*, 2006, **11**, 014006.
26 M. Tokunaga, N. Imamoto and K. Sakata-Sogawa, *Nat. Methods*, 2008, **5**, 159–161.
27 C. Konopka and S. Bednarek, *Plant J.*, 2008, **53**, 186–196.
28 G. Parikesit, J. Guasto, S. Girardo, E. Mele, R. Stabile, D. Pisignano, R. Lindken and J. Westerweel, *Biomicrofluidics*, 2009, **3**, 044111.